PROCEEDINGS OF THE ROYAL SOCIETY A MATHEMATICAL, PHYSICAL & ENGINEERING SCIENCES

# On the compaction of cohesive hyperelastic granules

T. I. Zohdi

*Proc. R. Soc. Lond. A* 2003 **459**, 1395-1401
doi: 10.1098/rspa.2003.1117

10.1098/rspa.2003.1117

THE ROYAL SOCIETY

# On the compaction of cohesive hyperelastic granules

By T. I. Zohdi

*Department of Mechanical Engineering, 6195 Etcheverry Hall, University of California, Berkeley, CA 94720-1740, USA*

*Received 21 March 2002; accepted 16 December 2002; published online 28 March 2003*

The compaction of cohesive hyperelastic polymeric granules is investigated. Finite strain concentration functions are developed for material models of compressible Mooney–Rivlin type, which allow one to analytically estimate, in fact rigorously bound, the progressive reduction of the volume fraction of the porous gap between the granules as a function of increasing applied loading.

**Keywords: hyperelasticity; cohesive granules; compaction; densification**

## 1. Introduction

Within the last decade, materials formed by compacted polymeric granules, such as Neopolen® P, a polypropylene foam, have become of increasing interest to industry due to their relatively easy formability and light weight. Such materials serve as packaging fillers, containers, shock absorbers and so forth (Tatzel 1996; Domas 1997). The usual process to manufacture such materials is to pack the polymeric granules into a container and then to compact them together (figure 1). A primary manufacturing interest is the estimation of the rate of densification, i.e. the reduction of the gap within the granular aggregate during compaction. The surfaces of individual granules are highly cohesive, therefore, if they meet under compression, they will immediately adhere. When full or nearly full densification is achieved, the material is then heated to the thermal-softening-threshold temperature in order to 'thermo-form' the final product. Clearly, before the thermo-forming process is initiated, it is desirable to attain full densification. The main objective of the present work is to estimate when this will occur as a function of the externally applied loading. We remark that, while there is considerable activity in the research of poro-plastic compaction of metallic powders (see Anand & Gu 2000; Gu *et al*. 2001; Akisanya *et al*. 1997; Fleck 1995; Brown & Abou-Chedid 1994), there is surprisingly little analysis of hyperelastic compaction at finite strains. Generally speaking, the compaction of metallic powders is closely related to the pioneering analysis of Gurson (1977), addressing void growth and coalescence at finite elasto-plastic strains. For the latest in the development of this widely used model we refer the reader to Pardoen & Hutchinson (2000).

Presently, the first phase in thermo-forming of hyperelastic granules, i.e. cold compaction to full densification, is investigated. The outline of the presentation is as follows. In § 2, material models of compressible Mooney–Rivlin type are introduced, and they are used to describe the responses of the individual granules. In § 3, a finite strain concentration function is derived, and it is used to develop a strict lower

 

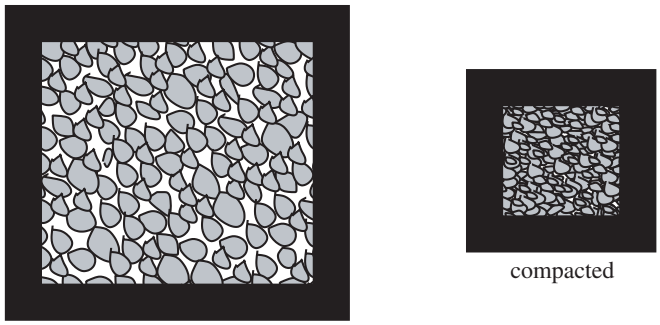


Figure 1. The compaction of cohesive granular pellets.

bound on the porous gap volume fraction in terms of the applied macroscopic loading. Finally, in § 4, examples illustrating the behaviour of the model are given.

## 2. A classical hyperelastic material model

A widely used class of mathematical representations for the constitutive response for hyperelastic polymeric materials under consideration are compressible Mooney–Rivlin stored energy functions of the form

$$W = \underbrace{K_1(\bar{\mathrm{I}}_C - 3) + K_2(\bar{\mathrm{II}}_C - 3)}_{\stackrel{\mathrm{def}}{=} \bar{W}} + \underbrace{\tfrac{1}{2}\kappa(\sqrt{\mathrm{III}_C} - 1)^2}_{\stackrel{\mathrm{def}}{=} U}. \tag{2.1}$$

Here $K_1 + K_2 = \frac{1}{2}\mu$, so that, in the infinitesimal deformation case, the response collapses to that of a linear isotropic Hookean solid and where $\boldsymbol{C} \stackrel{\mathrm{def}}{=} \boldsymbol{F}^{\mathrm{T}} \cdot \boldsymbol{F}$ is the right Cauchy–Green strain tensor, where $\boldsymbol{F} = \nabla_X \boldsymbol{x}$ is the deformation gradient, $\boldsymbol{u} = \boldsymbol{x} - \boldsymbol{X}$ is the displacement, $\boldsymbol{X}$ are referential coordinates, $\boldsymbol{x}$ are current coordinates,

$$\boldsymbol{S} = 2\frac{\partial W}{\partial \boldsymbol{C}} = J\boldsymbol{F}^{-1} \cdot \boldsymbol{\sigma} \cdot \boldsymbol{F}^{-\mathrm{T}}$$

is the second Piola–Kirchhoff stress, $\boldsymbol{\sigma}$ is the Cauchy stress and where $J$ is the Jacobian of $\boldsymbol{F}$, $J = \det \boldsymbol{F}$. In this material model, the first and second invariants of $\boldsymbol{C}$, $\mathrm{I}_C$ and $\mathrm{II}_C$ have been scaled by the square root of the third invariant, i.e.

$$\bar{\mathrm{I}}_C = \mathrm{I}_C \mathrm{III}_C^{-1/3} = \mathrm{I}_C J^{-2/3} \quad \text{and} \quad \bar{\mathrm{II}}_C = \mathrm{II}_C \mathrm{III}_C^{-2/3} = \mathrm{II}_C J^{-4/3},$$

to ensure that they contribute nothing to the compressible part of the response. This is motivated by defining an incompressible deformation gradient,

$$\bar{\boldsymbol{F}} \stackrel{\mathrm{def}}{=} J^{-1/3}\boldsymbol{F} = \mathrm{III}_C^{-1/6}\boldsymbol{F}$$

and

$$\bar{\boldsymbol{C}} \stackrel{\mathrm{def}}{=} \bar{\boldsymbol{F}}^{\mathrm{T}} \cdot \bar{\boldsymbol{F}} = J^{-2/3}\boldsymbol{C} = \mathrm{III}_C^{-1/3}\boldsymbol{C},$$

which leads to $\bar{J} = 1$. In other words, the corresponding scaled third invariant is always unity. The Cauchy stress can be split in the following manner, $\boldsymbol{\sigma} = \boldsymbol{\sigma}' + p\boldsymbol{1}$,

where $p \overset{\text{def}}{=} \frac{1}{3}\operatorname{tr}\boldsymbol{\sigma}$, and thus

$$\boldsymbol{S} = J\boldsymbol{F}^{-1}\cdot(\boldsymbol{\sigma}' + p\mathbf{1})\cdot\boldsymbol{F}^{-\mathrm{T}} = \underbrace{J\boldsymbol{F}^{-1}\cdot\boldsymbol{\sigma}'\cdot\boldsymbol{F}^{-\mathrm{T}}}_{\overset{\text{def}}{=}\boldsymbol{S}'} + Jp\boldsymbol{C}^{-1}. \tag{2.2}$$

We also have, by definition,

$$\boldsymbol{S} = 2\frac{\partial W}{\partial \boldsymbol{C}} = 2\frac{\partial \bar{W}}{\partial \boldsymbol{C}} + 2\frac{\partial U}{\partial \boldsymbol{C}} = 2\frac{\partial \bar{W}}{\partial \boldsymbol{C}} + 2\frac{\partial U}{\partial J}\frac{\partial J}{\partial \boldsymbol{C}} = \underbrace{2\frac{\partial \bar{W}}{\partial \boldsymbol{C}}}_{\boldsymbol{S}'} + \frac{\partial U}{\partial J}J\boldsymbol{C}^{-1}. \tag{2.3}$$

Since

$$\boldsymbol{\sigma}' = \frac{1}{J}\boldsymbol{F}\cdot\left(2\frac{\partial \bar{W}}{\partial \boldsymbol{C}}\right)\cdot\boldsymbol{F}^{\mathrm{T}},$$

equation (2.3) implies

$$p = \frac{\partial U}{\partial J} = \kappa(J-1). \tag{2.4}$$

## 3. Granular material densification

In order to perform a mesoscale analysis of the granular material, we represent the granules' elastic moduli, which are assumed to be isotropic, by the bulk and shear moduli, $\kappa_2$ and $\mu_2$. The porous 'material' (gap) is denoted by $\kappa_1$ and $\mu_1$, and is initially modelled as a soft (scaled) material, $\kappa_1 = \delta\kappa_2$ and $\mu_1 = \delta\mu_2$, where $\delta \ll 1$. Further remarks on this representation are made later in the analysis. Due to the assumption that the granular material becomes perfectly bonded upon contact, we can represent the solid phase as a continuous skeleton which surrounds the porous gap. In classical infinitesimal deformation analyses, macroscopic responses of materials that are heterogeneous on the mesoscale are described using a relation between averages,

$$\langle\boldsymbol{\sigma}\rangle_{\Omega_{\mathrm{o}}} = \mathbb{E}^*_{\mathrm{o}} : \langle\boldsymbol{\epsilon}\rangle_{\Omega_{\mathrm{o}}}, \quad \text{where } \langle\cdot\rangle_{\Omega} \overset{\text{def}}{=} \frac{1}{|\Omega_{\mathrm{o}}|}\int_{\Omega}\cdot\,\mathrm{d}\Omega_{\mathrm{o}},$$

and $\boldsymbol{\sigma}$ and $\boldsymbol{\epsilon}$ are the stress and infinitesimal strain tensor fields within a representative volume element (RVE) of (referential) volume $|\Omega_{\mathrm{o}}|$. If the effective property ($\mathbb{E}^*_{\mathrm{o}}$) is assumed isotropic, then one may write

$$\langle\boldsymbol{\sigma}\rangle_{\Omega_{\mathrm{o}}} = 3\kappa^*_{\mathrm{o}}\tfrac{1}{3}(\operatorname{tr}\langle\boldsymbol{\epsilon}\rangle_{\Omega_{\mathrm{o}}})\mathbf{1} + 2\mu^*_{\mathrm{o}}\langle\boldsymbol{\epsilon}'\rangle_{\Omega_{\mathrm{o}}},$$

where $\boldsymbol{\epsilon}' \overset{\text{def}}{=} \boldsymbol{\epsilon} - \frac{1}{3}(\operatorname{tr}\boldsymbol{\epsilon})\mathbf{1}$. We emphasize that quantities such as $\kappa^*_{\mathrm{o}}$ and $\mu^*_{\mathrm{o}}$ are not material properties, but are relations between averages, or more appropriately *apparent properties* (Huet 1990), which depend upon the averaging volume domain. For finite deformations, the effective property depends upon whether the averaging volume is taken to be the referential (undeformed) volume or the deformed configuration volume.

### (*a*) *A referential strain concentration function*

For the case of finite deformations, defining the *referential porous space volume fraction* by

$$v_{1\mathrm{o}} \overset{\text{def}}{=} \frac{|\Omega_{1\mathrm{o}}|}{|\Omega_{\mathrm{o}}|} = 1 - v_{2\mathrm{o}} = 1 - \frac{|\Omega_{2\mathrm{o}}|}{|\Omega_{\mathrm{o}}|},$$

we have by averaging over the referential configuration

$$\begin{aligned}\langle p\rangle_{\Omega_o} &= v_{1o}\langle p\rangle_{\Omega_{1o}} + v_{2o}\langle p\rangle_{\Omega_{2o}}\\ &= v_{1o}\kappa_1\langle J-1\rangle_{\Omega_{1o}} + v_{2o}\kappa_2\langle J-1\rangle_{\Omega_{2o}}\\ &= \kappa_1(\langle J-1\rangle_{\Omega_o} - v_{2o}\langle J-1\rangle_{\Omega_{2o}}) + v_{2o}\kappa_2\langle J-1\rangle_{\Omega_{2o}}\\ &= \underbrace{(\kappa_1 + v_{2o}(\kappa_2-\kappa_1)\,\mathcal{C}_o)}_{\kappa_o^*}\langle J-1\rangle_{\Omega_o}, \end{aligned} \tag{3.1}$$

where

$$\underbrace{\left(\frac{1}{v_{2o}}\frac{\kappa_o^*-\kappa_1}{\kappa_2-\kappa_1}\right)}_{\stackrel{\text{def}}{=}\mathcal{C}_o}\langle J-1\rangle_{\Omega_o} = \langle J-1\rangle_{\Omega_{2o}}. \tag{3.2}$$

$\mathcal{C}_o$ is a referential finite strain concentration function. *Once either* $\mathcal{C}_o$ *or* $\kappa_o^*$ *is known, the other can be determined.*

**Remark 3.1.** It almost goes without saying that, since $\langle p\rangle_{\Omega_o} = \kappa_o^*\langle J-1\rangle_{\Omega_o}$ must hold at infinitesimal and finite strains and since $J = \det \boldsymbol{F} = \det(\boldsymbol{1}+\nabla_X\boldsymbol{u}) \approx 1+\operatorname{tr}\nabla_X\boldsymbol{u}+\mathcal{O}(\nabla_X\boldsymbol{u}) = 1+\operatorname{tr}\boldsymbol{\epsilon}+\cdots$, at infinitesimal strains $\langle p\rangle_{\Omega_o} = \kappa_o^*\langle \operatorname{tr}\boldsymbol{\epsilon}\rangle_{\Omega_o}$. In other words, the effective bulk modulus in the reference configuration is the effective bulk modulus in the infinitesimal strain case, which, by definition, is posed over the undeformed reference configuration.

### (*b*) *A strict densification lower bound*

If a material sample, which is heterogeneous on the mesoscale, has the following prescribed loading on its *referential* surface, $\boldsymbol{u}|_{\partial\Omega_o} = \boldsymbol{L}\cdot\boldsymbol{X}$, then

$$\begin{aligned}\langle\nabla_X\boldsymbol{u}\rangle_{\Omega_o} &= \frac{1}{|\Omega_o|}\left(\int_{\Omega_{1o}}\nabla_X\boldsymbol{u}\,\mathrm{d}\Omega_{1o} + \int_{\Omega_{2o}}\nabla_X\boldsymbol{u}\,\mathrm{d}\Omega_{2o}\right)\\ &= \frac{1}{|\Omega_o|}\left(\int_{\partial\Omega_{1o}}\boldsymbol{u}\otimes\boldsymbol{N}\,\mathrm{d}A_{1o} + \int_{\partial\Omega_{2o}}\boldsymbol{u}\otimes\boldsymbol{N}\,\mathrm{d}A_{2o}\right)\\ &= \boldsymbol{L} + \frac{1}{|\Omega_o|}\int_{\partial\Omega_{1o}\cap\partial\Omega_{2o}}[\![\boldsymbol{u}]\!]\otimes\boldsymbol{N}\,\mathrm{d}A_{1o2}, \end{aligned} \tag{3.3}$$

where $(\boldsymbol{u}\otimes\boldsymbol{N} \stackrel{\text{def}}{=} u_iN_j)$ is a tensor product of the vector $\boldsymbol{u}$ and vector $\boldsymbol{N}$. $[\![\boldsymbol{u}]\!]$ describes the displacement jumps in the interfaces between $\Omega_{1o}$ and $\Omega_{2o}$. Since the material is fissure free, $\langle\nabla_X\boldsymbol{u}\rangle_{\Omega_o} = \boldsymbol{L}$, thus $\langle\boldsymbol{F}\rangle_{\Omega_o} = \boldsymbol{1}+\boldsymbol{L}$. For the Jacobian, we have

$$\langle J\rangle_{\Omega_o} = \frac{1}{|\Omega_o|}\int_{\Omega_o} J\,\mathrm{d}\Omega_o = \frac{|\Omega|}{|\Omega_o|}. \tag{3.4}$$

Under the special loading data $\boldsymbol{u}|_{\partial\Omega_o} = \boldsymbol{L}\cdot\boldsymbol{X}$, this result collapses to

$$\langle J\rangle_{\Omega_o} = \det(\boldsymbol{1}+\boldsymbol{L}). \tag{3.5}$$

The primary quantity of interest is the volume fraction of solid material, $v_2$, in the deformed configuration

$$v_2 \stackrel{\text{def}}{=} \frac{|\Omega_2|}{|\Omega|} = \frac{\langle J\rangle_{\Omega_{2o}}|\Omega_{2o}|}{\langle J\rangle_{\Omega_o}|\Omega_o|} = \frac{\langle J\rangle_{\Omega_{2o}}}{\langle J\rangle_{\Omega_o}}\,v_{2o}. \tag{3.6}$$

Explicitly, we have, by using the relationship in (3.2),

$$v_2 = \frac{\mathcal{C}_\mathrm{o}\langle J\rangle_{\Omega_\mathrm{o}} - \mathcal{C}_\mathrm{o} + 1}{\langle J\rangle_{\Omega_\mathrm{o}}} v_{2\mathrm{o}} = \left(\mathcal{C}_\mathrm{o} + \frac{1-\mathcal{C}_\mathrm{o}}{\langle J\rangle_{\Omega_\mathrm{o}}}\right) v_{2\mathrm{o}} = \left(\mathcal{C}_\mathrm{o} + \frac{1-\mathcal{C}_\mathrm{o}}{\det(\mathbf{1}+\boldsymbol{L})}\right) v_{2\mathrm{o}}. \tag{3.7}$$

As indicated earlier, once either $\mathcal{C}_\mathrm{o}$ or $\kappa_\mathrm{o}^*$ is known, the other can be determined. The approach taken is to use classical bounds on $\kappa_\mathrm{o}^*$ to generate bounds on $\mathcal{C}_\mathrm{o}$, which in turn can be used to bound the volume fraction of the solid material ($v_2$) in the deformed configuration. Specifically, we employ the Hashin & Shtrikman (1962, 1963) bounds for the effective bulk modulus in the reference configuration

$$\begin{aligned}\kappa_\mathrm{o}^{*-} &\stackrel{\mathrm{def}}{=} \kappa_1 + v_{2\mathrm{o}}\left(\frac{1}{\kappa_2-\kappa_1} + \frac{3(1-v_{2\mathrm{o}})}{3\kappa_1+4\mu_1}\right)^{-1} \leqslant \kappa_\mathrm{o}^* \\ &\leqslant \kappa_2 + (1-v_{2\mathrm{o}})\left(\frac{1}{\kappa_1-\kappa_2} + \frac{3v_{2\mathrm{o}}}{3\kappa_2+4\mu_2}\right)^{-1} \stackrel{\mathrm{def}}{=} \kappa_\mathrm{o}^{*+},\end{aligned} \tag{3.8}$$

where $\kappa_2 \geqslant \kappa_1$ and $\mu_2 \geqslant \mu_1$. Such bounds are the tightest possible on isotropic effective responses, with isotropic two-phase mesostructures, where only the volume fractions and phase contrasts of the constituents are known. For combinations where $\kappa_2 \gg \kappa_1$ and $\mu_2 \gg \mu_1$, and high volume fractions of the harder phase ($v_2$), it is well known that the Hashin–Shtrikman upper bound is quite accurate (Hashin 1983). Essentially, a continuous hard skeleton of material encompassing a softer phase (figure 1), exactly the case considered in this work, is a stiff mesostructure that is well characterized by the upper bound. Since $\kappa_\mathrm{o}^{*+} \geqslant \kappa_\mathrm{o}^*$, in compression we have $\mathcal{C}_\mathrm{o}(\kappa_\mathrm{o}^{*+}) \geqslant \mathcal{C}_\mathrm{o}(\kappa_\mathrm{o}^*)$ and thus, from (3.7), $v_2(\kappa_\mathrm{o}^{*+}) \leqslant v_2(\kappa_\mathrm{o}^*)$. In other words, our estimate of the volume fraction occupied by the solid in the deformed configuration, i.e. the densification, is a *strict lower bound*,

$$v_2(\kappa_\mathrm{o}^*) \geqslant \left(\mathcal{C}_\mathrm{o}(\kappa_\mathrm{o}^{*+}) + \frac{1-\mathcal{C}_\mathrm{o}(\kappa_\mathrm{o}^{*+})}{\det(\mathbf{1}+\boldsymbol{L})}\right) v_{2\mathrm{o}} = v_2(\kappa_\mathrm{o}^{*+}). \tag{3.9}$$

*Therefore, if the lower bound predicts full densification, $v_2(\kappa_\mathrm{o}^{*+}) \to 1$, then the true densification must tend to full densification, i.e. $v_2(\kappa_\mathrm{o}^*) \to 1$.* Also, it is important to remark that from (3.9) one sees that the rate of densification increases rapidly as the material becomes progressively more compressed.

**Remark 3.2.** Since $\kappa_\mathrm{o}^{*-} \leqslant \kappa_\mathrm{o}^*$, in compression we have $\mathcal{C}_\mathrm{o}(\kappa_\mathrm{o}^{*-}) \leqslant \mathcal{C}_\mathrm{o}(\kappa_\mathrm{o}^*)$ and thus, from (3.7), $v_2(\kappa_\mathrm{o}^{*-}) \geqslant v_2(\kappa_\mathrm{o}^*)$, leading to an upper bound on the volume fraction occupied by the solid in the deformed configuration:

$$v_2(\kappa_\mathrm{o}^*) \leqslant \left(\mathcal{C}_\mathrm{o}(\kappa_\mathrm{o}^{*-}) + \frac{1-\mathcal{C}_\mathrm{o}(\kappa_\mathrm{o}^{*-})}{\det(\mathbf{1}+\boldsymbol{L})}\right) v_{2\mathrm{o}} = v_2(\kappa_\mathrm{o}^{*-}). \tag{3.10}$$

*Consistent with the previous comments about the high accuracy of the lower densification bound, this upper bound is typically quite coarse and is of little practical value for the class of problems considered here.*

## 4. An example

Consider displacement data of the form ($t$ denotes time)

$$\boldsymbol{u}|_{\partial\Omega_\mathrm{o}} \stackrel{\mathrm{def}}{=} \begin{bmatrix} L_{11}\times t & 0 & 0 \\ 0 & L_{22}\times t & 0 \\ 0 & 0 & L_{33}\times t \end{bmatrix} \begin{bmatrix} X_1 \\ X_2 \\ X_3 \end{bmatrix}. \tag{4.1}$$

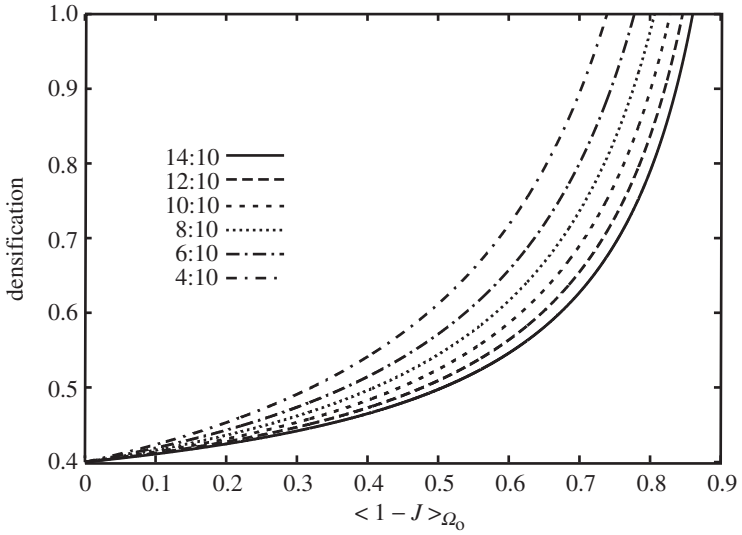


Figure 2. The lower bound on the volume fraction occupied by the solid, $v_2(\kappa_o^{*+})$, for various $\mu_2/\kappa_2$ ratios.

The displacement-controlled loading rate was $L_{11} = L_{22} = L_{33} = -0.1$, leading to $\langle 1-J\rangle_{\Omega_o} = 1-(1+L_{11}t)(1+L_{22}t)(1+L_{33}t) = 1-(1-0.1t)^3$. Here there are no rate effects; time simply serves as a parameter to drive the simulations. The bulk modulus of the granules was fixed at $\kappa_2 = 10$ GPa and the shear modulus, $\mu_2$, was varied, owing to the wide range of such values used in industrial applications. The starting volume fraction value was $v_2(t=0) = v_{2o} = 0.4$. Simulations were repeatedly rerun with progressively smaller values of the porous space stiffness reduction factor ($\delta$), forcing $\delta \to 0$. Beyond a threshold of $\delta = 0.001$ the results were insensitive, and thus the simulations can be considered to be 'convergent' to simulations involving true voids. As indicated by (3.9), the densification rate increases rapidly with increasing load (figure 2). By increasing shear modulus, more pressure is required to compress the material and densification is delayed. At full densification, we have $|\Omega_1| = 0$, and thus

$$\langle J\rangle_{\Omega_o} = \frac{|\Omega|}{|\Omega_o|} = \frac{|\Omega_1| + |\Omega_2|}{|\Omega_o|} = \frac{|\Omega_2|}{|\Omega_o|}. \tag{4.2}$$

Since $|\Omega_o| = |\Omega_{1o}| + |\Omega_{2o}|$ and $1 = v_{1o} + v_{2o}$, we have $|\Omega_{1o}| = (1 - v_{2o})|\Omega_o|$ and thus an expression for the total volumetric deformation of the granular phase

$$\frac{|\Omega_2|}{|\Omega_{2o}|} = \frac{\langle J\rangle_{\Omega_o}|\Omega_o|}{|\Omega_o| - |\Omega_{1o}|} = \frac{\langle J\rangle_{\Omega_o}|\Omega_o|}{v_{2o}|\Omega_o|} = \frac{\langle J\rangle_{\Omega_o}}{v_{2o}}. \tag{4.3}$$

From figure 2, we observe that, for $\mu_2/\kappa_2 = 14/10$, full densification occurs at approximately $\langle 1 - J\rangle_{\Omega_o} = 0.86$, leading to $|\Omega_2|/|\Omega_{2o}| = 0.35$, while for $\mu_2/\kappa_2 = 4/10$, full densification occurs at $\langle 1 - J\rangle_{\Omega_o} = 0.73$, yielding $|\Omega_2|/|\Omega_{2o}| = 0.675$.

## 5. Concluding remarks

The primary result in this communication was a lower bound on the volume fraction occupied by solid granules undergoing compaction, in the deformed configuration, as

a function of the external applied loading. Central to the result was the development of a finite-strain concentration function bound built upon the Hashin–Shtrikman upper bound, whose high accuracy in representing effective responses for mesostructures formed by a continuous hard skeleton of material encompassing a softer phase, exactly the case considered in this work, is well known. Once the effective bulk modulus was accurately described in the reference configuration, all subsequent results followed from purely geometric arguments.

The author thanks Professor David Steigmann for his helpful comments during the preparation of this article.

## References

Akisanya, A. R., Cocks, A. C. F. & Fleck, N. A. 1997 The yield behavior of metal powders. *Int. J. Mech. Sci.* **39**, 1315–1324.

Anand, L. & Gu, C. 2000 Granular materials: constitutive equations and shear localization. *J. Mech. Phys. Solids* **48**, 1701–1733.

Brown, S. & Abou-Chedid, G. 1994 Yield behavior of metal powder assemblages. *J. Mech. Phys. Solids* **42**, 383–398.

Domas, F. 1997 Eigenschaftprofile und Anwendungsübersicht von EPE und EPP. Technical report of the BASF Company, Ludwigshafen, Germany.

Fleck, N. A. 1995 On the cold compaction of powders. *J. Mech. Phys. Solids* **43**, 1409–1431.

Gu, C., Kim, M. & Anand, L. 2001 Constitutive equations for metal powders: application to powder-forming processes. *Int. J. Plasticity* **17**, 147–209.

Gurson, A. L. 1977 Continuum theory for ductile rupture by void nucleation and growth. I. Yield criteria and flow rules for porous media. *J. Engng Mater. Technol.* **99**, 2–15.

Hashin, Z. 1983 Analysis of composite materials: a survey. *ASME J. Appl. Mech.* **50**, 481–505.

Hashin, Z. & Shtrikman, S. 1962 On some variational principles in anisotropic and nonhomogeneous elasticity. *J. Mech. Phys. Solids* **10**, 335–342.

Hashin, Z. & Shtrikman, S. 1963 A variational approach to the theory of the elastic behaviour of multiphase materials. *J. Mech. Phys. Solids* **11**, 127–140.

Huet, C. 1990 Application of variational concepts to size effects in elastic heterogeneous bodies. *J. Mech. Phys. Solids* **38**, 813–841.

Pardoen, T. & Hutchinson, J. W. 2000 An extended model for void growth and coalescence. *J. Mech. Phys. Solids* **48**, 2467–2512.

Tatzel, H. 1996 Grundlagen der Verarbeitungstechnik von EPP-Bewährte und neue Verfahren. Technical report of the BASF Company, Ludwigshafen, Germany.